A measurement of the ratio of the nucleon structure function in copper and deuterium

European Muon Collaboration

J. Ashman[12], B. Badelek[16,a], G. Baum[18,b], J. Beaufays[2,c], C.P. Bee[7], C. Benchouk[8], I.G. Bird[5,d], S.C. Brown[7,e], M.C. Caputo[18,f], H.W.K. Cheung[10,g], J.S. Chima[11,h], J. Ciborowski[16,a], R. Clifft[11], G. Coignet[6], F. Combley[12], G. Court[7], G. d'Agostini[8], J. Drees[17], M. Düren[1], N. Dyce[5], A.W. Edwards[17,i], M. Edwards[11], T. Ernst[3], M.I. Ferrero[13], D. Francis[7], E. Gabathuler[7], J. Gajewski[16], R. Gamet[7], V. Gibson[10,j], J. Gillies[10,k], P. Grafström[14,1], K. Hamacher[17], D. von Harrach[4,m], P. Hayman[7], J.R. Holt[7], V.W. Hughes[18], A. Jacholkowska[2,n], T. Jones[7], E.M. Kabuss[4,m], B. Korzen[17], U. Krüner[17], S. Kullander[14], U. Landgraf[3], D. Lanske[1], F. Lettenström[14,o], T. Lindqvist[14], M. Matthews[7], Y. Mizuno[4,p], K. Mönig[17], F. Montanet[8], J. Nassalski[15,q], T. Niinikoski[2], P.R. Norton[11], F.G. Oakham[11,r], R.F. Oppenheim[18,s], A.M. Osborne[2], V. Papavassiliou[18], N. Pavel[17,t], C. Peroni[13], H. Peschel[17,u], R. Piegaia[18,f], B. Pietrzyk[8], B. Povh[4], P. Renton[10], J.M. Rieubland[2], K. Rith[4], E. Rondio[16,a], L. Ropelewski[16,a], D. Salmon[12,k], A. Sandacz[15,q], T. Schröder[3], K.P. Schüler[18], K. Schultze[1], T.-A. Shibata[4], T. Sloan[5], A. Staiano[13], H.E. Stier[3+], J. Stock[3], G.N. Taylor[10,v], J.C. Thompson[11], T. Walcher[4,m], J. Toth[6,w], L. Urban[1], L. Urban[6,w], W. Wallucks[3], S. Wheeler[12,1], W.S.C., Williams[10], S.J. Wimpenny[7,x], R. Windmolders[9], J. Womersley[10,y], K. Ziemons[1]

[1] III Physikalisches Institut A, Physikzentrum,RWTH, D-5100 Aachen, Germany
[2] CERN, CH-1211 Geneva 23, Switzerland
[3] Fakultät für Physik, Universität Freiburg, D-7800 Freiburg, Germany
[4] Max-Planck-Institut für Kernphysik, 6900 Heidelberg, Germany*
[5] Department of Physics, University of Lancaster, Lancaster LA1 4YB, UK
[6] Laboratoire d'Annecy-le-Vieux de Physique des Particules, BP110, F-74019 Annecy-le-Vieux, Cedex, France
[7] Department of Physics, University of Liverpool, Liverpool L69 3BX, UK
[8] Centre de Physique des Particles, Faculté des Sciences de Luminy, F-13288 Marseille, France
[9] Faculté des Sciences, Université de Mons, B-7000 Mons, Belgium
[10] Nuclear Physics Laboratory, University of Oxford, Oxford OX1 3RH, UK
[11] Rutherford and Appleton Laboratory, Chilton, Didcot OX11 0QX, UK
[12] Department of Physics, University of Sheffield, Sheffield S3 7RH, UK
[13] Istituto di Fisica, Universitá di Torino, I-10125, Italy
[14] Department of Radiation Science, University of Uppsala, S-75121 Uppsala, Sweden
[15] Institute for Nuclear Studies, 00681 Warsaw, Poland**
[16] Physics Institute, University of Warsaw, 00681 Warsaw, Poland***
[17] Fachbereich Physik, Universität Wuppertal, D-5600 Wuppertal, Germany
[18] Physics Department, Yale University, New Haven, CT06516, USA

[a] University of Warsaw, Poland, partly supported by CPBP-01.06
[b] Permanent address, University of Bielefeld, Germany
[c] Now at TRASYS, Brussels, Belgium
[d] Now at NIKHEF-K, AJ Amsterdam, The Netherlands
[e] Now at TESA. S.A., Renens, Switzerland
[f] Now at City University, Buenos Aires, Argentina
[g] Now at University of Colorado, Boulder, Colorado, USA
[h] Now at British Telecom, London, UK
[i] Now at Jet, Joint Undertaking, Abingdon, UK
[j] Now at University of Cambridge, Cambridge, UK
[k] Now at R.A.L., Chilton, Didcot, UK
[l] Now at CERN, Geneva, Switzerland
[m] Now at University of Mainz, Mainz, Germany
[n] Now at L.A.L., Orsay, France
[o] Now at University of California, Santa Cruz, USA
[p] Now at Osaka University, Osaka, Japan
[q] Permanent address, Institute for Nuclear Studies, Warsaw, Poland
[r] Now at NRC, Ottawa, Canada
[s] Now at AT&T, Bell Laboratories, Naperville, Ill. USA
[t] Now at University of Hamburg, Hamburg, Germany
[u] Now at Gruner and Jahr AG, Itzehoe, Germany
[v] Now at University of Melbourn, Parkville, Victoria, Australia
[w] Permanent address: Central Research Institute for Physics, Budapest, Hungary
[x] Now at University of California, Riverside, USA
[y] Now at University of Florida, Gainesville, USA
[+] Deceased

Abstract. Results are presented on the ratios of the nucleon structure function in copper to deuterium from two separate experiments. The data confirm that the nucleon structure function, F_2, is different for bound nucleons than for the quasi-free ones in the deuteron. The redistribution in the fraction of the nucleon's momentum carried by quarks is investigated and it is found that the data are compatible with no integral loss of quark momenta due to nuclear effects.

1 Introduction

In 1983, the EMC published results which showed that the nucleon structure function in a nuclear target is not the same as that in a quasi-free nucleon in deuterium. This result, now referred to as the EMC effect, was largely unpredicted, and gave rise to considerable experimental and theoretical interest. After the initial publication [1], the effect was soon confirmed by a reanalysis of old data from SLAC [2], and subsequently by new experiments at CERN [3] and SLAC [4] using both charged and neutral lepton beams. The EMC's original result was obtained by taking the ratios of the nucleon structure function measured in two separate experiments, and hence was subject to some degree of systematic uncertainty [5]. Subsequent measurements were made by the EMC which reduced such errors and the results on part of the available data have already been published [6]. In this paper we report the measurements from the complete data sample and also the results from a second independent measurement comparing data from copper and deuterium. Further details of this work can be found in [7–11]. More recently the NMC have published high precision measurements of the ratios for He:D, C:D, Ca:D [12], C:Li, Ca:Li and Ca:C [13] and comparison is made with the data presented here.

2 The formalism of deep inelastic scattering

The double differential cross-section for unpolarised charged lepton deep inelastic scattering (D.I.S.) from a nucleon can be written in the one photon exchange approximation in terms of the two structure functions F_1^N and F_2^N

$$\frac{d^2\sigma(x,Q^2)}{dQ^2\,dx} = \frac{4\pi\alpha^2}{Q^4}\left[\left(1-y-\frac{Mxy}{2E}\right)\right.$$
$$\left. \times \frac{F_2^N(x,Q^2)}{x} + y^2 F_1^N(x,Q^2)\right] \qquad (2.1)$$

with the variables defined in Table 1. The structure functions themselves are related by the ratio, $R^N(x,Q^2)$, of the absorption cross sections for longitudinally and transversely polarised virtual photons, σ_l and σ_t respectively

$$2xF_1^N(x,Q^2) = \frac{F_2^N(x,Q^2)}{1+R^N(x,Q^2)}\left(1+\frac{4M^2x^2}{Q^2}\right). \qquad (2.2)$$

Table 1. The variables of deep inelastic scattering

M	Proton rest mass
E	Energy of incident muon
$E'\,(p'_\mu)$	Energy (momentum) of scattered muon
θ	Muon scattering angle
ν	$E-E'$, energy of virtual photon in the lab
q	Four momentum transfer
$Q^2 = -q^2 \cong 4\,EE'\sin^2(\theta/2)$	(Invariant mass)^2 of virtual photon
$x = Q^2/2M\nu$	Bjorken scaling variable
$y = \nu/E$	Bjorken scaling variable
$W^2 = 2M\nu + M^2 - Q^2$	(Hadronic energy)^2 in centre of mass

Recent measurements have shown that R^N is independent of the nuclear atomic mass, A [14], thus allowing the ratio of structure functions F_2 for different targets to be equated to the ratio of the measured cross-sections.

3 The experimental arrangement

The experiments were performed in the muon beam line at the CERN SPS using the EMC forward spectrometer [15] to detect the scattered muon and the fast forward hadrons produced in D.I.S. The spectrometer and the analysis procedures for this phase of the experiment have already been described [16, 17]. Figure 1 shows a schematic diagram of the spectrometer. Two separate measurements were performed in which data from different nuclear and deuterium targets were taken. In the first measurement the targets were interchanged frequently. In the second experiment the data were taken from copper and deuterium targets simultaneously. Since the data from the nuclear and deuterium targets were taken at about the same time the major potential systematic errors present in the original EMC measurement [1, 5] were eliminated.

The first of the two experiments, from which part of the data have already been published [6], used targets of He, C, Cu, Sn and D_2 which were situated about 1 m downstream of the polarised target. This experiment ran concurrently with the polarised target experiment [16, 17], taking approximately 10% of the data. The arrangement of the targets which were mounted on a moving chariot is shown in Fig. 2a. We refer to this as the "chariot experiment". Each target occupied the same region of space with respect to the spectrometer, the targets being interchanged at intervals of about one hour. In this way, the acceptance of the apparatus was the same for each target, and it cancels to a good approximation when measuring the cross section ratio from the event yields. The muon flux incident on each target was measured as described in [18].

In the second experiment, hereinafter referred to as the "addendum experiment", the polarised target [16, 17] was replaced by the target assembly shown in Fig. 2b.
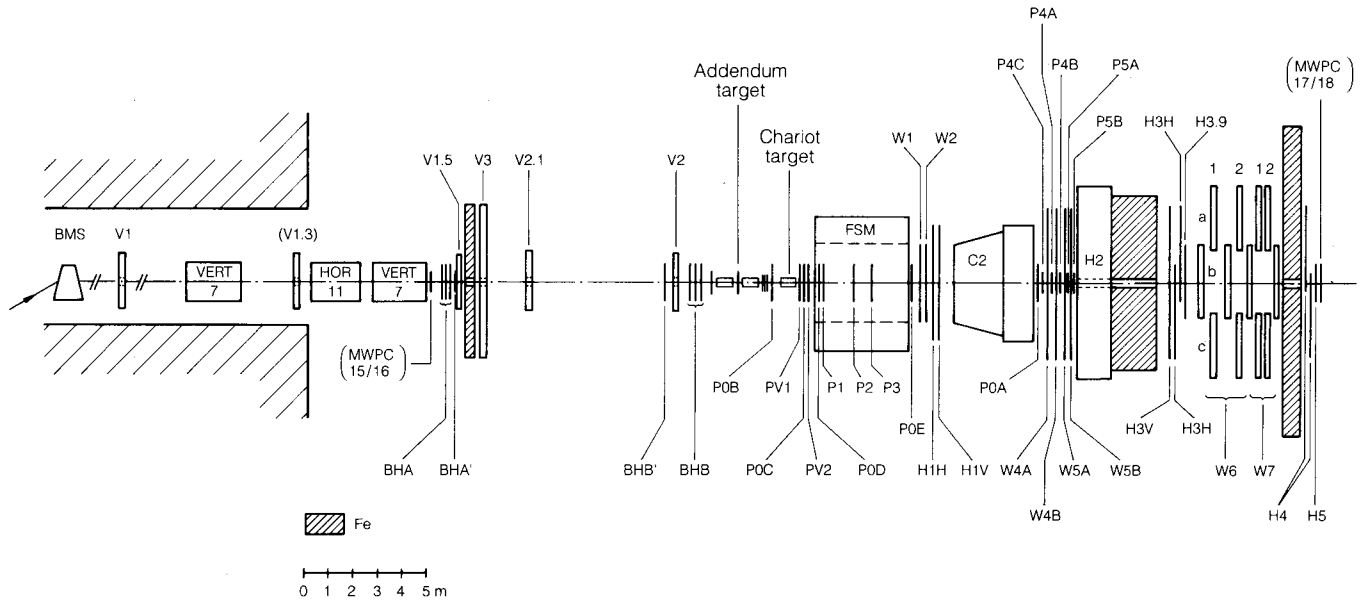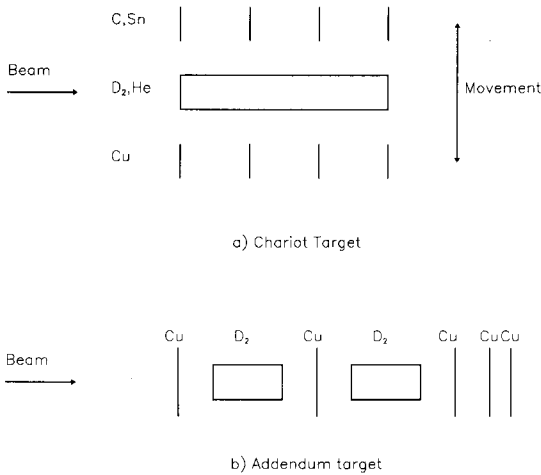
Fig. 1. Schematic diagram of the spectrometer

Fig. 2. Schematic diagram of the two target arrangements

Here, targets of Cu and D_2 were disposed alternately in the beam, the chariot targets remaining in position downstream. Figure 3 shows the distribution of the vertex coordinate along the beam direction from one experimental run when the chariot Cu target was in position. Good separation of events from the different targets was achieved. In the addendum set-up, each target sees the same flux of muons, and this cancels in the ratio. However, in contrast to the chariot experiment, the acceptance is different for Cu and D_2, and to obtain the cross section ratio a correction must be applied. The two experiments thus are complementary each eliminating one important systematic error. The characteristics of the targets are given in Table 2.

4 The analysis of the data

The experiment was operated at incident muon energies of 100, 120 and 200 GeV for the chariot target and at 100 and 280 GeV for the addendum targets. The data were

Table 2. The characteristics of the targets

Chariot Target

Target	D2	He	C	Cu	Sn
Density ρ (g/cm^3)	0.162 ± 0.001	0.124 ± 0.001	2.265	8.965	7.310
Thickness t (cm)	59.8 ± 0.3	59.0 ± 0.3	3.667	0.895	1.160
ρt (g/cm^2)	9.69 ± 0.08	7.42 ± 0.07	8.306	8.024	8.480

Addendum target

Target	Cu(1)	D_2(1)	Cu(2)	D_2(2)	Cu(3)	Cu(4)	Cu(5)
Density ρ (g/cm^3)	8.96	0.162 ± 0.001	8.96	0.162 ± 0.001	8.96	8.96	8.96
Thickness t (cm)	0.907	99.8 ± 0.3	0.907	99.8 ± 0.3	0.302	0.303	0.302
ρt (g/cm^2)	8.127	16.2 ± 0.1	8.127	16.2 ± 0.1	2.706	2.715	2.706

Table 3. Kinematic cuts on the chariot data

Nominal beam energy (GeV)	100	120	200	280
Beam energy (GeV)	75–125	105–135	175–225	245–315
$Q^2 (\text{GeV}/c)^2$	> 2	> 2	> 3	> 3
v (GeV)	> 10	> 10	> 25	> 25
p'_μ (GeV/c)	> 20	> 20	> 30	> 40
θ (mrad)	> 10			
y	< 0.65 for $0.02 \leq x < 0.04$			
	< 0.75 for $0.04 \leq x < 0.06$			
	< 0.85 for $0.06 \leq x < 0.7$			
Number of events remaining	34 297	38 077	34 019	6 926

passed through a chain of analysis programmes in which pattern recognition, track and vertex reconstruction were carried out.

For the chariot data the cuts shown in Table 3 were applied to remove regions where radiative corrections were large, where acceptance was rapidly varying, where resolution smearing was large or where significant backgrounds existed from pion decay. The ratios of the event yields per unit muon flux from each nuclear target to deuterium were then taken in bins of x. To obtain the ratio of the nucleon structure function for each nuclear target to that in deuterium various corrections were applied. Radiative corrections (< 1% over most of the x range rising rapidly to 8% at the smallest x values) were applied using the exact formalism of Mo and Tsai [19]. Small corrections (< 1%) were also made for the neutron excess in the larger nuclei using the simple parameterisation $\dfrac{F_2^n}{F_2^p} = (0.92 - 0.86 x) \pm 0.05$ which is compatible with the recent high precision NMC measurements [20]. Other small corrections ($\sim 0.1\%$) were applied for the material in the end caps of the D_2 target and the air between the nuclear targets. In addition a correction was

made for the 1% admixture of H_2 in the D_2. Monte Carlo studies were made to study the possibility of differences in the software reconstruction efficiencies for the different targets due to background hits confusing the reconstruction programmes [21]. No difference could be found and so corrections were unnecessary.

For the addendum data, the disposition of the targets was different than for the chariot and so slightly different cuts (shown in Table 4) were applied. The ratio of the yield from the nuclear to deuterium targets were obtained using the number of events reconstructed in each target location from the reconstructed vertex position (Fig. 3). Normalisation to the muon flux was unnecessary since the muon beam passed through all the targets simultaneously. A correction was needed for the number of events
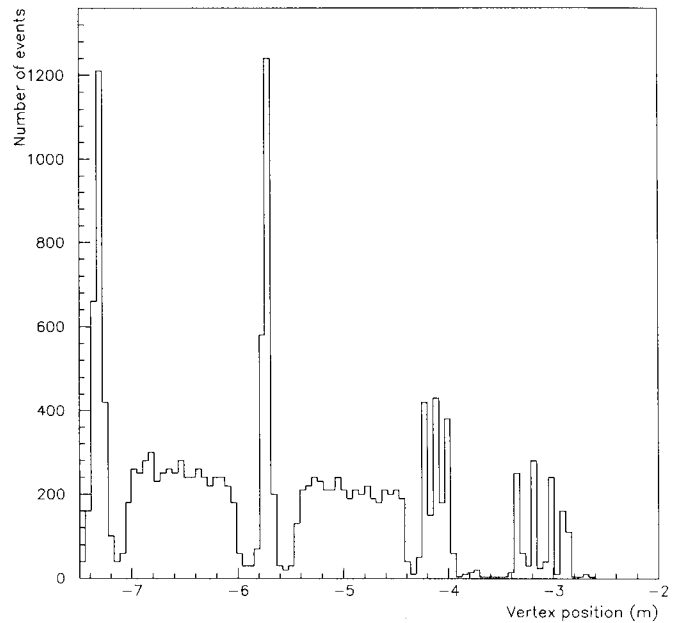
Fig. 3. Reconstructed vertex distribution along the beam direction; the events from each target are clearly identifiable

**Table 4.** Kinematic cuts on the addendum data

Nominal beam energy (GeV)	100	280
Beam energy range (GeV)	75–125	245–315
v (GeV)	> 10	> 25
p'_μ (GeV/c)	> 20	> 40
θ (mrad)	> 15	
y	< 0.55 for $0.01 \leq x < 0.02$	
	< 0.65 for $0.02 \leq x < 0.04$	
	< 0.75 for $0.04 \leq x < 0.06$	
	< 0.85 for $0.06 \leq x < 0.8$	
$Q^2 (\text{GeV}/c)^2$	2– 5 for $0.02 \leq x < 0.04$	10– 17 for $0.02 \leq x < 0.04$
	2–10 for $0.04 \leq x < 0.06$	10– 31 for $0.04 \leq x < 0.06$
	2–17 for $0.06 \leq x < 0.15$	17– 55 for $0.06 \leq x < 0.15$
	4–17 for $0.15 \leq x < 0.2$	17–105 for $0.15 \leq x < 0.3$
	4–31 for $0.2 \leq x < 0.3$	
	6–31 for $0.3 \leq x < 0.4$	31–195 for $0.3 \leq x < 0.8$
	10–31 for $0.4 \leq x < 0.5$	
	17–55 for $0.5 \leq x < 0.8$	
Number of events	235 388	71 880

Table 5a. Results from the chariot experiment

x	$\langle Q^2 \rangle$ (GeV/c)^2	μ_{Cu}/σ_{D2}	Stat. error	Syst. error
0.031	4.5	0.930	0.025	0.022
0.050	8.5	0.955	0.020	0.019
0.079	13.6	0.996	0.016	0.018
0.123	18.1	1.047	0.019	0.019
0.173	21.3	1.021	0.022	0.018
0.244	24.7	1.037	0.021	0.019
0.342	30.0	0.945	0.029	0.017
0.443	34.4	0.957	0.045	0.018
0.563	40.4	0.910	0.096	0.017

Table 5b. Results from the addendum experiment

x	$\langle Q^2 \rangle$ (GeV/c)^2	σ_{Cu}/σ_{D2}	Stat. error	Syst. error
0.015	4.5	0.857	0.022	0.023
0.031	3.3	0.963	0.013	0.018
0.050	6.4	1.005	0.012	0.013
0.079	8.5	1.011	0.011	0.011
0.123	11.0	1.041	0.016	0.010
0.173	16.1	1.031	0.012	0.011
0.243	19.3	1.018	0.014	0.010
0.343	25.8	0.962	0.021	0.011
0.444	36.0	0.959	0.034	0.013
0.612	46.4	0.918	0.043	0.013
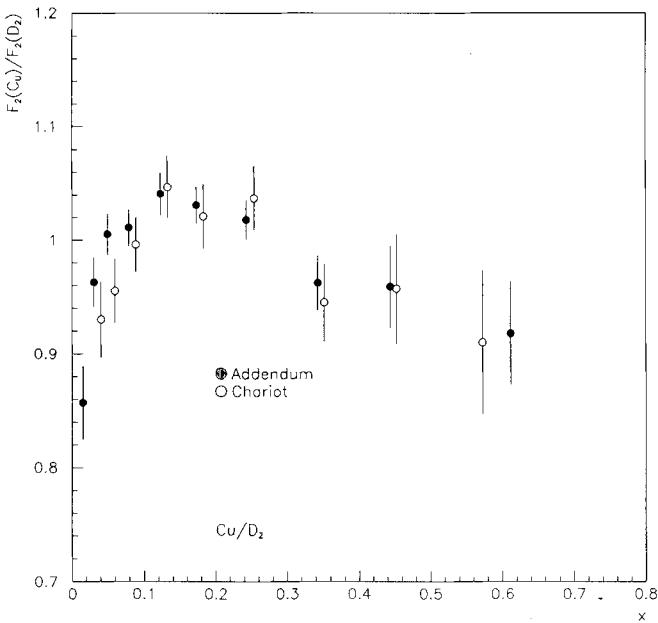
Fig. 4. The measured structure function ratios $F_2(\text{Cu})/F_2(\text{D})$ for the data from each target arrangement as a function of x

smeared by experimental resolution from the copper to deuterium and vice versa. This was found to be $\sim 0.3\%$ by fitting a Breit Wigner shape to the distributions of the vertex coordinate from each target along the beam direction and extrapolating the tails into the adjacent targets. In addition, a correction ($\sim 3\%$) was necessary for the variation of the acceptance along the beam direction.

The correction was deduced in each bin by assuming a parabolic variation of the acceptance with vertex position. This was shown to be a reasonable assumption using a Monte Carlo simulation. A fit of a parabolic acceptance variation with the ratio of the yield per nucleon from copper to deuterium as a further free parameter was performed in each bin. The result gave the ratio of the yield per nucleon in copper to that in deuterium. The corrections described for the chariot data were then applied to obtain the ratio of the nucleon structure functions in copper and deuterium. Again Monte Carlo studies showed that the software reconstruction efficiency was the same for copper as that for deuterium and no correction was applied.

The radiative corrections become very large for $x < 0.02$, using the techniques described above due to the large contribution from coherent elastic scattering on heavy nuclei with accompanying radiative photons. Such large corrections incur large systematic errors. To avoid this effect for $x < 0.02$, events were selected with an accompanying hadron for the measurement of the structure function ratio [10]. The residual radiative correction on the ratio is then reduced to $\sim 2\%$ in this region and is principally due to the inelastic tail. The calorimeter H_2 (Fig. 1) was used to reject electrons from conversion of radiated photons by demanding that the ratio of the energy deposited by a track in the electromagnetic section to the total energy is less than 0.8 [7, 10].

5 Results

The measured ratios of the structure functions for Cu : D from the two experiments are given in Tables 5a and b and shown as a function of x in Fig. 4. The systematic errors were derived from studies of the sensitivity to the cuts, from the uncertainties in the fits to the acceptance variation for the addendum experiment and from the relative uncertainties of the muon flux measurement for the chariot experiment. There is good agreement between the measurements from the two experiments and the averaged results are given in Table 6 and shown in Fig. 5. Here the statistical and systematic errors have been combined. The data in Fig. 5 show that the ratios lie below unity at small x, with a rise above unity at intermediate x and a further

Table 6. Merged chariot addendum ratio

x	σ_{Cu}/σ_{D2}	Error
0.015	0.857	0.032
0.031	0.953	0.018
0.050	0.990	0.015
0.079	1.006	0.013
0.123	1.043	0.016
0.173	1.029	0.014
0.243	1.023	0.015
0.343	0.956	0.020
0.444	0.958	0.029
0.612	0.915	0.037

fall below unity at large x. Such behaviour is compatible with previous observations [6, 12, 13, 22]. Many theoretical models have been proposed to explain the ratios of the nucleon structure function measured in nuclear and deuterium targets (for a review see [23]). The predictions of three such models [24–26] which are applicable over the whole x range are shown in Fig. 5. It can be seen that these models reproduce qualitatively the main features of the data.

A comparison with other high Q^2 experiments is shown in Fig. 6 where the ratios are plotted as a function of A, the target nucleus atomic weight. The ratios He:D, C:D and Ca:D were taken from [12] and Sn:D from [6], whilst the Li:D ratio was taken from [13]. There is a reasonably continuous behaviour between the data presented here and the measurements in references [6, 12, 13]. The straight lines are fits of the form CA^α and Fig. 7 shows the values of C and α as a function of x, compared to the lower Q^2 data from SLAC [4]. Again there is reasonable agreement with the SLAC data, showing that any Q^2 dependence of the ratios must be small. The NMC data also showed only weak, if any, Q^2 dependence [12] and studies of the Q^2 dependence of the ratios in this experiment [9] did not reveal any significant variation. It can be seen from Fig. 7 that there exists a relatively strong A dependence at small x, the so called shadowing region, so that the nucleon structure function decreases with A. At intermediate x, the so called antishadowing region, the A dependence is weaker with a possible increase with A. At higher x a decrease of the structure function with A is indicated. Figure 6 shows that the ratio is well represented by the form CA^α.

In the quark parton model of the nucleon the data in Fig. 5 imply that there is a decrease in the momentum carried by quarks in the shadowing region and at high x and an increase in the antishadowing region. The quantity

Fig. 6. The structure function ratio as a function of target atomic weight, A. The Cu data are from this experiment (solid circles); the Sn data from [6] and the data at lower A from NMC [12, 13] (open circles). The curves are the results of the fits of the form CA^α
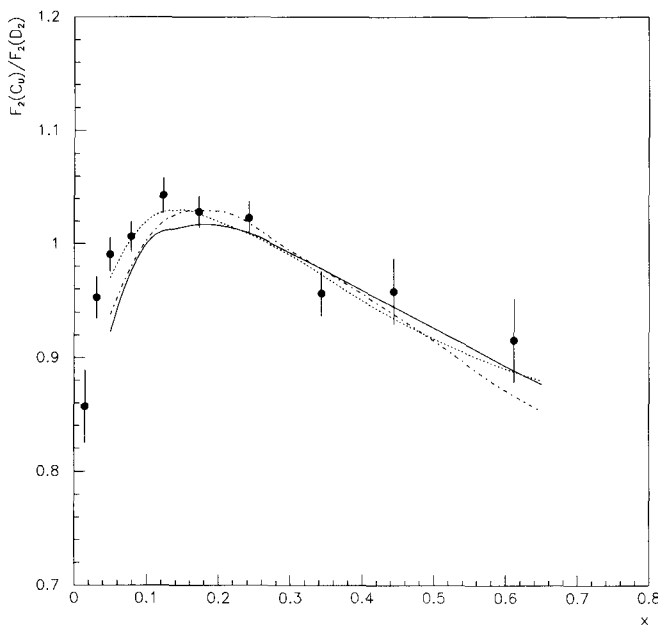

Fig. 5. The averaged structure function ratios for copper as a function of x; the smooth curves represent the predictions of theoretical models (solid curve, Close et al. [24]; dotted curve, Zhu [25]; dash dotted curve Guaglie et al. [26])
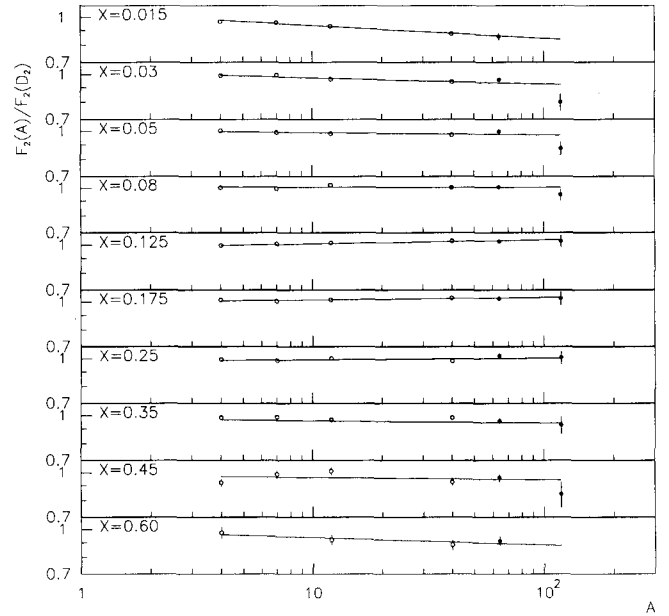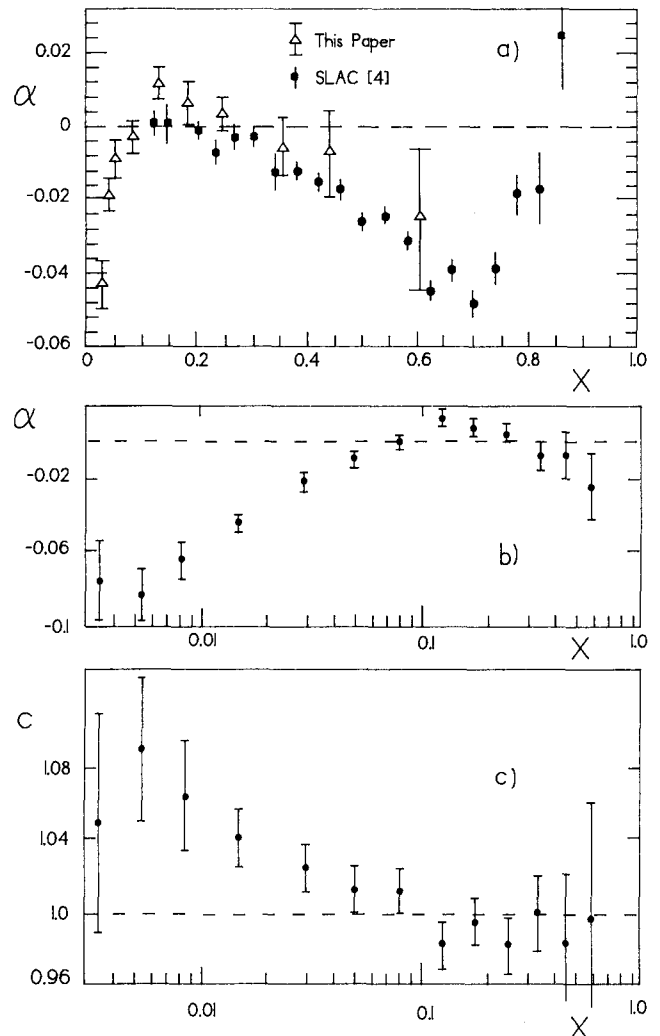
Fig. 7a–c. The coefficients C and α from the fits CA^α in Fig. 6, as a function of x; a α, together with the SLAC measurements [4]; b α, from this experiment; c C, from this experiment

$\frac{18}{5}\int_{x_1}^{x_2}\left(\frac{F_2^A}{F_2^D}-1+f_m\right)F_2^D K_2\,dx$ represents the change due to nuclear effects in the total fraction of the nucleon's momentum carried by quarks in the range $x_1 < x < x_2$. The total fraction of the nucleon's momentum carried by quarks is found to be about 0.5 from the available data [27]. In this integral F_2^A and F_2^D are the nucleon structure functions measured in nuclear and deuterium targets, respectively, f_m is a small correction for nuclear binding effects [28] and K_2 is a target mass correction [29] which is close to unity in this kinematic range. The NMC [12] studied these integrals and found that they were compatible with zero both over the whole x range of the data and also when the range is restricted to the shadowing and antishadowing regions. This implies, in the quark parton model, that momentum compensation is occurring.

Figure 8 shows the values of these integrals evaluated separately for the shadowing region, defined as $x_{\min} < x < 0.06$ where $x_{\min}$ is the lowest value of x of the available data, the antishadowing region defined as $0.06 < x < 0.3$ and the high x region defined as $x > 0.31$. The integrals are plotted as a function of A using the ratios from [12,13] for He, Li, C and Ca, those presented here for Cu and from [6] for Sn and from the SLAC data [4,30] for the high x region together with values of F_2^D from the recent NMC parameterisation. There is some momentum change unaccounted for due to the unmeasured region below $x_{\min}$. This was estimated to be ~ 0.0005 for low A [12, 13] and ~ 0.0015 for Cu by as-

suming that the ratio $\frac{F_2^A}{F_2^D}$ in the unmeasured region is similar in value to the first measured bin. Such saturation of the ratio has redently been observed [32]. The contribution below $x_{\min}$ has been neglected, although the difference in $x_{\min}$ for the EMC and NMC data mainly explains the fluctuation in the copper integral (Fig. 8b).

It can be seen from Fig. 8 that the momentum changes increase with A with much larger changes in the shadowing and antishadowing regions than in the high x range. In fact the change in the high x region is almost negligible compared to the changes in the shadowing and antishadowing regions. Thus the momentum compensation in the shadowing and antishadowing regions is almost complete. This is illustrated further in Fig. 9 where the total integrals over the shadowing and antishadowing regions are shown ($x_{\min} < x < 0.3$). The mean value over all the measurements is found to be 0.0010 ± 0.0004 and is compatible with zero allowing for the unmeasured momentum change for $x < x_{\min}$.

The parton fusion picture [31] would predict a value zero for the integral over the shadowing and antishadowing range since, in this model, shadowing is produced by the fusion of very soft partons from different nucleons in the nucleus to make harder partons. Thus by momentum conservation a depletion in the momentum fraction in the shadowing region will be compensated by an increase in the antishadowing region. This is compatible with the data as described above and as such it is evidence for the parton fusion picture. However, the argument is
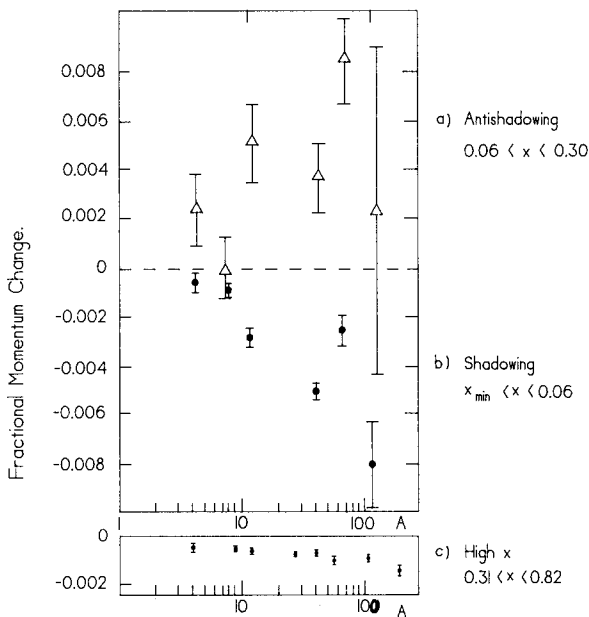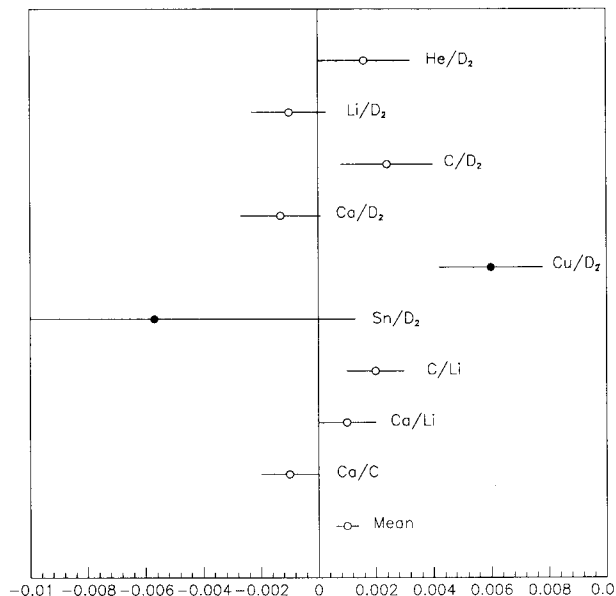

Fig. 8a–c. The integrals $\frac{18}{5}\int_{x_{\min}}^{x_{\max}}\left(\frac{F_2^A}{F_2^D}-1+f_m\right)F_2^D K_2\,dx$ as a function of A; **a** Antishadowing region (triangles) $0.06 < x < 0.30$. The low A data are from [12, 13], the copper data are from this experiment, the Sn data from [6]. **b** Shadowing region (points) ($x_{\min} < x < 0.06$) where $x_{\min}$ is the lowest value of x for the available data. **c** High x region $0.31 < x < 0.82$ using the SLAC data [4, 30]

Fig. 9. The total integral over the range $x_{\min} < x < 0.30$ for all the available data [6, 12, 13 and this experiment]. The lower point shows the mean value, which is compatible with zero as discussed in the text

not completely conclusive since the possibility cannot be excluded that the observed momentum compensation is accidental. It is possible that shadowing and antishadowing could be produced by two different mechanisms, which accidentally make equal contributions to the integrals in the two regions.

6 Conclusions

The ratios of the nucleon structure functions in copper and deuterium measured using the total data sample from the final stage of the EMC experiment have been presented. Comparison with data from other experiments shows that the A dependence is well represented by the form CA^{α} with C and α varying with x. Comparison of the shadowing and antishadowing regions shows that the decrease in the total momentum fraction carried by the quarks in the shadowing region at small x is the same as the increase in the antishadowing region at intermediate x. The momentum changes at high x are much smaller. The data therefore indicate the possibility of momentum compensation between the shadowing and antishadowing regions. The changes in the momentum fraction in each region tend to increase with A.

References

1. EMC, J.J. Aubert et al.: Phys. Lett. 123B (1983) 275
2. A. Bodek et al.: Phys. Rev. Lett. 50 (1983) 1431; A. Bodek et al.: Phys. Rev. Lett. 51 (1983) 534
3. BCDMS, G. Bari et al.: Phys. Lett. 163B (1985) 282; A.C. Benvenuti et al.: Phys. Lett. B189 (1987) 483
4. SLAC, E-139 R.G. Arnold et al.: Phys. Rev. Lett. 52 (1984) 727
5. EMC, J.J. Aubert et al.: Nucl. Phys. B293 (1987) 740
6. EMC, J. Ashman et al.: Phys. Lett. 202B (1988) 603
7. J.D. Gillies: D. Phil. Thesis. University of Oxford (1988), RALT-077
8. H. Peschel: Ph.D. Thesis. University of Wuppertal (1990)
9. L. Ropelewski: Ph.D. Thesis. University of Warsaw (in preparation)
10. A. Staiano: Ph.D. Thesis. University of Heidelberg (1989)
11. J. Ashman: PhD Thesis. University of Sheffield (1988)
12. NMC, P. Amaudruz et al.: Z. Phys. C51 (1991) 387
13. NMC, P. Amaudruz et al.: Z. Phys. C53 (1992) 73
14. SLAC, E140, S. Dasu et al.: Phys. Rev. Letts. 60 (1988) 2591
15. O.C. Allkofer et al.: Nucl. Instrum. Methods 179 (1981) 445
16. EMC, J. Ashman et al.: Phys. Lett. 206B (1988) 364
17. EMC, J. Ashman et al.: Nucl. Phys. B328 (1989) 1
18. R. Mount: Nucl. Instrum. Methods 187 (1981) 401
19. L. Mo, Y.S. Tsai: Rev. Mod. Phys. 41 (1969) 205; Y.S. Tsai: SLAC-PUB-848 (1971)
20. NMC, D. Allasia et al.: Phys. Lett. B249 (1990) 366
    NMC, P. Amaudraz et al.: Nucl. Phys. B371 (1992) 3
21. H.W.K. Cheung: D. Phil. Thesis. University of Oxford (1987) RALT-055
22. M. Arneodo et al.: Phys. Lett. 211B (1988) 493; M. Arneodo et al.: Nucl. Phys. B333 (1990) 1
23. L. Frankfurt, M. Strikman: Phys. Rep. 160 (1988) 235
    R.J.M. Covalan, E. Predazzi: Problems of fundamental modern physics. Singapore: World Scientific 1991
    M.Arneodo: CERN PPE92-113 (to be published in Phys. Rep.)
24. F.E. Close, R.G. Roberts, G. Ross: Phys. Lett. 168B (1986) 400; F.E. Close, R.G. Roberts: Phys. Lett. 213B (1988) 91
25. W. Zhu: Phys. Lett. 235B (1990) 170
26. L. Guaglie, C. Zhijun, Z. Chasheng: Beijing preprint BIHEP-TH-89-29 (1989)
27. T. Sloan, G. Smadja, R. Voss: Phys. Rep. 162 (1988) 45
28. M. Arneodo: Ph.D. Thesis. University of Princeton (1992)
29. O. Nachtmann: Nucl. Phys. B78 (1974) 455
30. The reanalysed version of the data in [4] was used for Fig. 8 see A. Bodek: Proc. of the Lepton-Photon Symposium and Europhysics Conference LP-HEP 91. Geneva (1991)
31. N.N. Nikolaev, V.I. Zacharov: Phys. Lett. B55 (1975) 397
32. E665, M.R. Adams et al.: Fermilab-Pub-92/51-E